This is the Pre-Published Version.

This manuscript version is made available under the CC-BY-NC-ND 4.0 license (https://creativecommons.org/licenses/by-nc-nd/4.0/)

The following publication Xie, K., Guo, M., Lu, W., & Huang, H. (2014). Aligned TiO2 nanotube/nanoparticle heterostructures with enhanced electrochemical performance as three-dimensional anode for lithium-ion microbatteries. Nanotechnology, 25(45), 455401 is available at https://doi.org/10.1088/0957-4484/25/45/455401.

Aligned TiO_2 Nanotube/Nanoparticle Heterostructure with Enhanced Electrochemical Performance as 3D anode for Lithium-Ion Microbatteries

Keyu Xie[a,*], Min Guo[b], Haitao Huang[b,*]

[a] *State Key Laboratory of Solidification Processing and School of Materials Science and Engineering, Northwestern Polytechnical University, Xi'an, 710072, China*

[b] *Department of Applied Physics and Materials Research Centre, The Hong Kong Polytechnic University, Hong Kong, China*

* Corresponding author.

Tel:+86-029-88460361; E-mail: nwpuxky@163.com (K.Y. Xie)

Tel: +852-2766-5694; E-mail: aphhuang@polyu.edu.hk (H. Huang)

Abstract: A novel TiO_2 three-dimensional (3D) anode with aligned TiO_2 nanotube/nanoparticle heterostructure (TiO_2 NT/NP) was developed by simply immersing as-anodized TiO_2 NTs into water, and further crystallized by post-annealing. The heterostructure, with the core in a tubular morphology and both the outer and inner surfaces consisting of nanoparticles, was confirmed by FESEM

and TEM. A reversible areal capacity of 0.126 mAh·cm^{-2} was retained after 50 cycles for the TiO_2 NT/NP heterostructure electrode, which was higher than that of the TiO_2 NT electrode (0.102 mAh·cm^{-2} after 50 cycles). At the current densities of 0.02, 0.04, 0.06, 0.08, 0.10, and 0.20 mA·cm^{-2}, the areal capacities were 0.142, 0.127, 0.117, 0.110, 0.104, and 0.089 mAh·cm^{-2}, respectively, for the TiO_2 NT/NP heterostructure electrode. The corresponding areal capacities were 0.123, 0.112, 0.105, 0.101, 0.094, and 0.083 mAh·cm^{-2}, respectively, for the the TiO_2 NT electrode. The enhenced electrochemical performance was attributed to the unique microstructure of the TiO_2 NT/NP heterostructure electrode with the TiO_2 NT cores being straight pathways for electronic transport and TiO_2 NPs offering enhanced surface areas for lithium-ion insertion/extraction. The results described here inspire a facile approach to the fabrication of a 3D anode with enhanced electrochemical performance for lithium-ion microbattery applications.

Keywords: Anodization; Water Treament; TiO_2 Nanotube/Nanoparticle Heterostructure; 3D Anode; Lithium-Ion Microbatteries.

Highlights:

1. A 3D TiO_2 NT/NP heterostructure electrode is developed by a facile method.
2. Both the areal capacity and the rate capability of the electrode are enhanced.
3. The heterostructure plays a key role to the improved electrochemical performance.

1. Introduction

Lithium-ion batteries (LIBs) are used in a wide range of applications, from micro- or nano-electromechanical systems (MEMSs/NEMSs) to portable electronic devices, and even to the hybrid vehicles and renewable energy systems[1, 2]. Very recently, in order to meet the ever increasing demand on both high energy and high power densities of LIBs, three-dimensional (3D) nanoarchitectured electrode has received a great deal of attention in academia and industry[3, 4]. To date, 3D nanoarchitectured electrodes with large surface areas and short paths for Li^+ diffusion and electron transport are widely fabricated by anodization, lithography, template-synthesis and 3D printing methods, respectively[5-11]. Among these methods, anodization is proven to be a simple, reliable, highly controllable, and low-cost method that can be scaled up for the preparation of sophisticated 3D nanoarchitectured electrodes directly on conductive metal substrates for lithium-ion microbattery (LIMB) applications[12-14].

A series of anodic metal oxide or hydroxide, such as TiO_2, Fe_2O_3, $Ni(OH)_2$, V_2O_5 and Co_3O_4[15-19], has been explored as 3D nanoarchitectured electrodes, and have displayed enhanced performance for electrochemical energy storage. Among them, anodic TiO_2 nanotube (TiO_2 NT) array has been considered as one of the most promising 3D anode materials for LIMBs, due to its high Li^+ intercalation voltage plateau, which is helpful to avoid the decomposition of organic electrolyte, the formation of solid electrolyte interface (SEI) film and the occurrence of lithium dendrites on the electrode under high charge-discharge rate, as well as structural

stability during lithium-ion insertion/extraction for long-cycle stability[20-22]. Though the unique spatial-structure of highly ordered TiO_2 NTs offers intrinsic high surface area, wich facilitates the transport of lithium-ions between the TiO_2 and electrolyte interface, as well as the smooth and straight superhighways to electron transport, the rate capability of TiO_2 NTs is still hindered by the semiconducting nature of TiO_2, leading to slow transportation of electrons, and low kinetic properties at the electrode/electrolyte interface[23-25]. The reported specific capacities of TiO_2 electrodes generally lie within 77-322 $mAh \cdot g^{-1}$, and are strongly influenced by the morphology and crystal structure of the materials[26-28].

As a consequence, great efforts have been carried out to further enhance the electrochemical performances of 3D nanoarchitectured TiO_2 NT electrodes recently. The most common strategy to achieve the high charge-discharge rate of 3D TiO_2 NT electrodes is to improve their electronic conductivity by: (1) coating conductive components, such as Ag[29]; (2) doping with metal or non-metal, such as Sn[20], H[23] or N[30]; (3) introducing Ti^{3+} species with oxygen vacancies[23, 31, 32]. While taking the modest areal capacity of TiO_2 NT electrodes into account, active electrode materials with large specific capacity, such as MoO_3[33], Fe_2O_3[34], SnO_2[35], Cu_6Sn_5[36] and Sn[37], are uauslly deposited onto the TiO_2 NT electrodes to obtain high areal capacity of these 3D nanoarchitectured TiO_2 NT composite electrodes. To construct these composite electrodes, various methods, including radio-frequency magnetron sputtering[37], electrodepositon[38], sol-gel[39], and solvethermal method[35], have to be used to deposit active electrode materials onto

the TiO_2 NTs. Nevertheless, to a certain degree, these fabrication processes are not so convenient for practical applicaitons. Hence, a facile and economic route to enhance both the rate capability and areal capacity of 3D TiO_2 NT based electrode is highly desired.

Herein, we report a facile synthesis of a novel TiO_2 3D anode with aligned TiO_2 nanotube/nanoparticle heterostructure (TiO_2 NT/NP) for LIMB applications. The aligned TiO_2 NT/NP heterostructure is developed by simply immersing as-anodized TiO_2 NTs into water, and further crystallized by annealing at 400 °C. Compared to its TiO_2 NT counterpart, such a hierarchical architecture exhibits superior electrochemical performance, with the TiO_2 NT core providing a straight pathway for fast electron transport and the surface TiO_2 NPs offering enhanced surface area for lithium-ion insertion/extraction. As a result, the TiO_2 NT/NP heterostructure electrodes are expected to show high energy and high power densities. Meanwhile, the facile and economic synthesis route is also promising for large-scale production and offers new opportunities for exploring 3D electrodes with enhanced electrochemical performance.

2. Experimental

2.1 Materials

Titanium foils (99.7%) were purchased from Strem Chemical (USA). Ethylene glycol (EG, 99.5%), ammonium fluoride (96%), acetone, and ethanol were obtained from International Laboratory (USA). Deionized (DI) water (18.2 MΩ·cm) was

produced by Direct-Q 3 Water Purification Systems (Millipore).

2.2 Fabrication of TiO_2 NT/NP composite electrodes

Prior to anodization, Ti foils were first degreased by ultrasonication in cold acetone, ethanol and DI water, respectively, and followed by drying in pure N_2 stream. The TiO_2 NT arrays were then fabricated by a potentiostatic anodization (working area: 1.0×1.0 cm^2) for 10 min at room temperature using an electrolyte consisting of 0.5 wt% ammonium fluoride in an aqueous EG solution (3 vol% DI water in EG). The anodization was carried out in a two-electrode electrochemical cell with platinum foil as the cathode and the Ti foil as the anode under a constant DC voltage of 60 V using a computer controlled source meter (Model 2400, Keithley, USA). Only one side of the Ti foil surface was exposed to the electrolyte and the other one was covered by an electroplater's tape. After anodization, the TiO_2 NTs were taken out and immersed in water. Finally, the water-treated TiO_2 NT/NP heterostructure was annealed in a tube furnace (TZF, Carbolite) in air at 400 °C for 2 h to crystallize the TiO_2 NTs/NPs. In this study, TiO_2 NTs (without water treatement) of the same thickness as that of TiO_2 NTs/NPs, were also prepared and annealed for comparison.

2.3 Characterizations

The morphology of the samples was examined by field-emission scanning electron microscope (FESEM, JEOL JSM-6335F) at an accelerating voltage of 5.0 kV. X-ray diffraction (XRD) was conducted by a Bruker D8 advance diffractometer (Philips) with Cu Kα radiation (λ=1.54 Å) operating at 40.0 kV and 40.0 mA. Transmission

electron microscopy (TEM) images were captured on a JEM-2010 (JEOL) microscope at an accelerating voltage of 200 kV. Samples for TEM observation were prepared by dispersing the nanotube array in ethanol under ultrasonication, followed by drying on a Cu grid.

2.4 Electrochemical measurements

To evaluate the electrochemical behaviour of these composite electrodes, 2032-coin type cells with the TiO_2 NT/NP heterostructure electrodes or TiO_2 NT electrodes as the working electrode (area=1 cm^2), lithium foil as the counter and reference electrodes, and Celgard 2400 as the separator were assembled in a glove box filled with Ar gas. The electrolyte consisting of a solution of 1.0 M $LiPF_6$ in ethylene carbonate (EC)/dimethyl carbonate (DMC) (1:1 in volume) was obtained from Shenzhen Kejing Instrument Co. Ltd.

The cycle performance was evaluated on Land CT2001A tester in a voltage range of 1.0 to 2.8 V (vs. Li^+/Li) at a constant current density of 0.02 $mA \cdot cm^{-2}$. The rate capacity was tested at 0.02, 0.04, 0.06, 0.08, 0.10, and 0.20 $mA \cdot cm^{-2}$, respectively. Cyclic voltammetry (CV) was measured with a scan rate of 0.1 $mV \cdot s^{-1}$ in a voltage range of 1.0 to 2.8 V by using an electrochemical workstation (CHI 660C, CH Instruments, Inc. USA) for these cells. Electrochemical impedance spectroscopy (EIS) was measured in the frequency range of 100 kHz to 0.01 Hz with an ac perturbation voltage of 5 mV.

3. Results and discussion

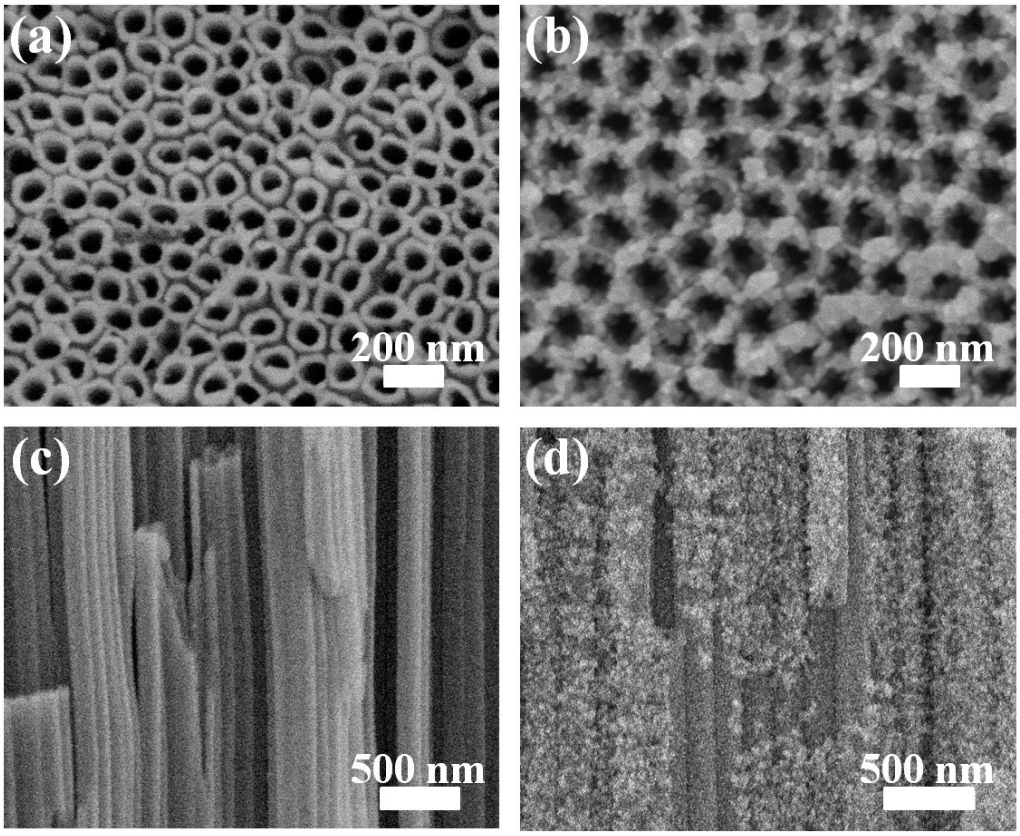

Fig. 1. (a), (c) FESEM top view and cross-sectional images of as-anodized TiO_2 NTs, respectively; (b), (d) FESEM top view and cross-sectional images of TiO_2 NTs/NPs, respectively.

Fig. 1a and 1c show the microstructure of the TiO_2 NTs obtained by potentiostatic anodization in the EG-based electrolyte containing of 0.5 wt% NH_4F and 3 vol% DI water. It can be seen that, after anodization, highly ordered and well separated TiO_2 NT array with smooth tube walls was grown directly on metallic Ti foil substrate. Each nanotube with an average outer diameter of ~130 nm and wall thickness of ~20 nm can be clearly seen. While after water immersion for 3 days, the tube morphology and microstructure changed greatly. The top mouths of as-anodized TiO_2 NTs were

smooth (Fig. 1a). However, they became rough with small nanoparticles accumulated on the top surface after water immersion (Fig.1b). Furthermore, due to the accumulated nanoparticles, which were emerged from both the inner and outer sides of the TiO_2 NTs, the separated top mouths of TiO_2 NTs were merged together, and the inner diameter of TiO_2 NTs was decreased. In addition, these small nanoparticles were also anchored on the sidewalls of the TiO_2 NTs, as shown in Fig. 1d.

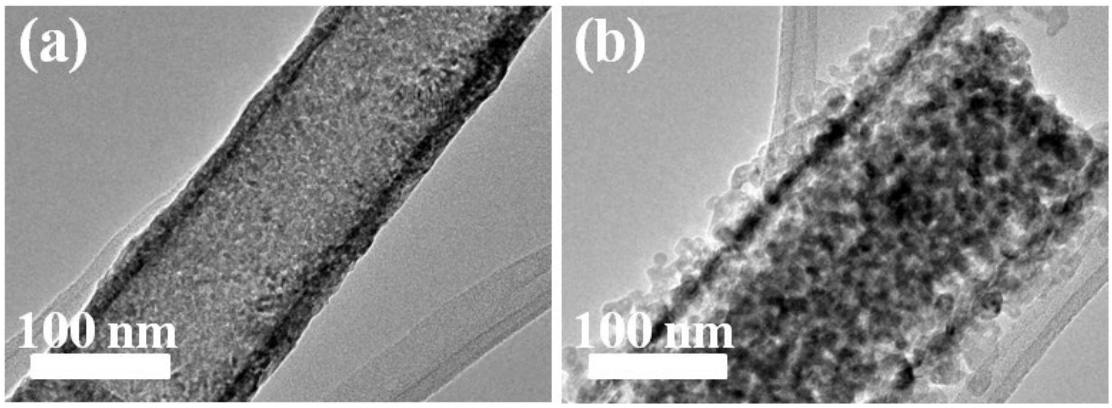

Fig. 2. TEM images of (a) as-anodized TiO_2 NT and (b) TiO_2 NT/NP.

Transmission electron microscopy (TEM) images of as-anodized TiO_2 NT and TiO_2 NT/NP further clarify the detailed morphology and microstructure conversion before and after water treatment. As can been seen in Fig.2a and 2b, the sidewall of TiO_2 NT became thinner after water immersion for 3 days, and both outer and inner sides of the tube wall were anchored with nanoparticles. The gradually thinning of tube sidewalls indicated that the TiO_2 NT/NP heterostructure was formed by consuming the tube walls and converting them to nanoparticles[40]. The possible reason for this phenomenon is that a dissolution-precipitation process assisted by

water may take place at the tube wall surface of the as-anodized TiO_2 NTs, where some fluorides may still be remained after anodization[41, 42]. Therefore, the TiO_2 NT/NP heterostructure was developed via the water treatment of the as-anodized TiO_2 NTs.

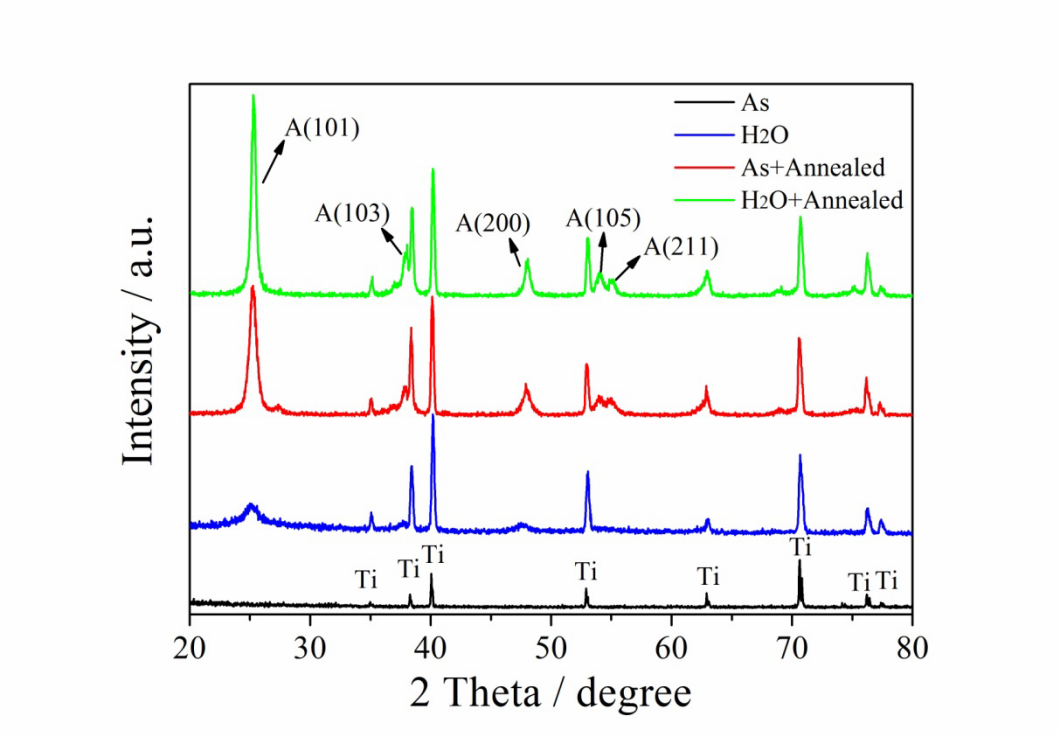

Fig. 3. XRD patterns of TiO_2 NTs with different post-treatment processes. As: as-anozied TiO_2 NTs without water treatment; H_2O: as-anozied TiO_2 NTs with water treatment; As+Annealed: as-anozied TiO_2 NTs after annealing at 400 °C for 2 h; H_2O+Annealed: water-treated TiO_2 NTs after annealing at 400 °C for 2 h; A: anatase; Ti: titanium. The Ti peaks originated from the underlying substrate.

As shown in Fig. 3, the phase transformation of the TiO_2 NT-based electrodes during the fabrication process was examined by X-ray diffraction (XRD). The XRD patterns show that the as-anodized TiO_2 NTs were amorphous in nature and were

partially crystallized into anatase for TiO_2 NT/NP heterostructure after immersion in water for 3 days, according to the emerged broad anatase (101) and (200) peaks. When the two samples were annealed in air, anatase became the dominant phase. Clearly, the broader anatase (101) diffraction peak for the water-treated sample after post-annealing indicated the smaller average crystalline size, compared to the annealed TiO_2 NTs without water treatment. As a consequence, the surface area of TiO_2 NT/NP heterostructure has increased to about twice that of TiO_2 NTs, according to our previous results[40]. In this case, an enhanced surface area for lithium-ion insertion/extraction of the TiO_2 NT/NP heterostructure electrode have been formed.

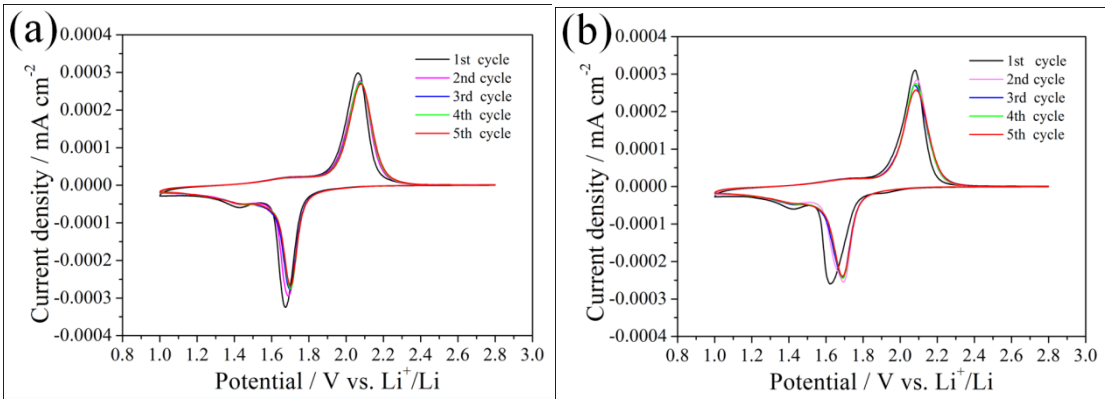

Fig. 4. CV curves of annealed (a) TiO_2 NTs and (b) TiO_2 NT/NP heterostructure as anode at a scan rate of 0.1mV s^{-1} for the first five cycles within a potential range of 1.0 to 2.8 V (vs. Li/Li^+).

Fig. 4a and 4b show the CV curves of the annealed TiO_2 NTs and TiO_2 NT/NP heterostructure electrode at a scan rate of 0.1 $mV \cdot s^{-1}$, respectively. A pair of pronounced cathodic and anodic peaks around 1.7 and 2.1 V (vs. Li^+/Li) is observed,

due to the electrochemical insertion/extraction of Li^+ from the crystalline anatase TiO_2, respectively. The overall reaction of TiO_2 with Li^+ can be written as :

$$TiO_2 + xLi^+ + xe^- \leftrightarrow Li_xTiO_2 \quad (1)$$

where the x is known to be ca. 0.5 for anatase TiO_2[24, 43]. It should be noted that, besides the first cycle, the CV curves of the two electrodes in four subsequent cycles almost completely overlap, indicating a good reversibility and stability of these TiO_2-based electrodes, consistent with previous reports[20-22].

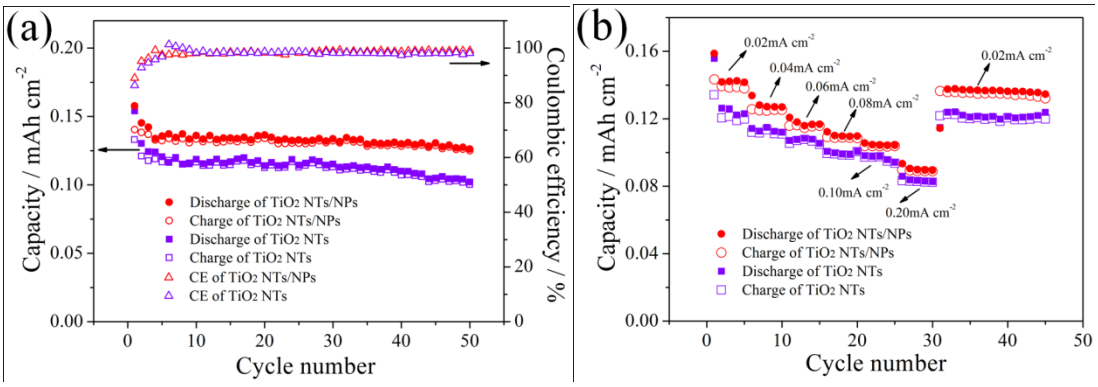

Fig. 5. (a) Areal capacities and Coulombic efficiency as a function of cycle number for TiO_2 NTs and TiO_2 NT/NP heterostructure electrodes at a current density of 0.02 $mA \cdot cm^{-2}$; (b) rate capability plots for TiO_2 NTs and TiO_2 NT/NP heterostructure electrodes at different current densities of 0.02, 0.04, 0.06, 0.08, 0.10, and 0.20 $mA \cdot cm^{-2}$.

The electrochemical behaviour of lithium insertion/extraction in TiO_2 NT/NP heterostructure was evaluated by galvanostatic cycling tests and compared to that of TiO_2 NTs as shown in Fig. 5a. It is seen that, for the TiO_2 NT/NP heterostructure

electrode, the first discharge areal capacity was 0.158 mAh·cm^{-2} and the Coulombic efficiency was about 89.0%, while they were 0.154 mAh·cm^{-2} and 86.4%, respectively, for the TiO_2 NT electrode at a current density of 0.02 mA·cm^{-2}. Furthermore, after the areal capacity gradually decreased in the first 5 cycles, a reversible capacity of 0.126 mAh·cm^{-2} was retained after 50 cycles for the TiO_2 NT/NP heterostructure electrode, which is slightly higher than that of the TiO_2 NTs electrode (0.102 mAh·cm^{-2} after 50 cycles). The enhanced areal capacity of TiO_2 NT/NP heterostructure electrode may be attributed to the improved surface pseudocapacitive Li^+ storage[44], which was derived from the increased surface area of TiO_2 NTs with water treatment. In addition, both the TiO_2 NT/NP heterostructure and TiO_2 NT electrodes exhibit stable cyclic performance with a Coulombic efficiency above 98% after the first 10 cycles.

Fig. 5b shows the areal capacities of the TiO_2 NT/NP heterostructure and TiO_2 NT electrodes at various current rates. With the incremental increase in the current rates of 0.02, 0.04, 0.06, 0.08, 0.10, and 0.20 mA·cm^{-2}, the measured areal capacities were 0.142, 0.127, 0.117, 0.110, 0.104, and 0.089 mAh·cm^{-2} (according to the 5th, 10th, 15th, 20th, 25th, and 30th discharge areal capacity in Fig. 5b), respectively, for the TiO_2 NT/NP heterostructure electrode, compared to areal capacities of 0.123, 0.112, 0.105, 0.101, 0.094, and 0.083 mAh·cm^{-2}, respectively, for the the TiO_2 NT electrode at the same current rates. The rate capability measurements of the two electrodes clearly demonstrate that the TiO_2 NT/NP heterostructure electrode exhibits a better rate performance than its counterpart.

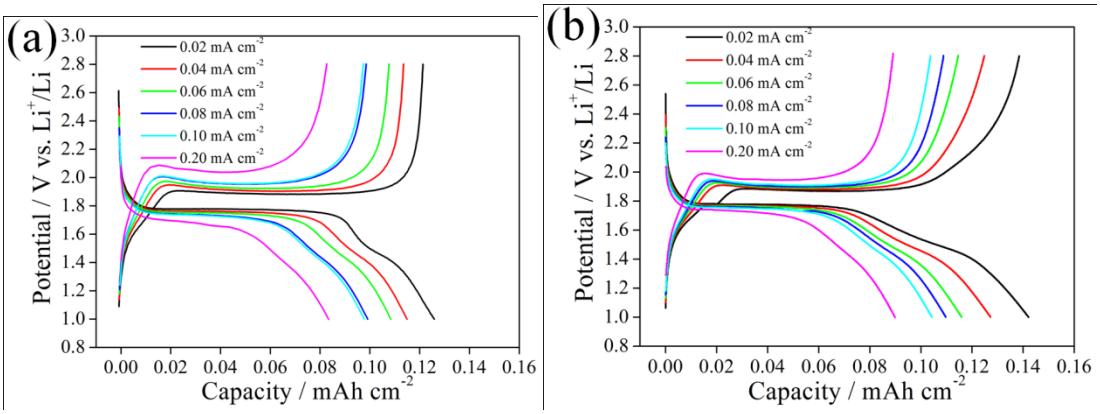

Fig. 6. Charge/discharge profiles of annealed (a) TiO_2 NT and (b) TiO_2 NT/NP heterostructure electrodes at different current densities. The black, red, green, blue, cyan, and magenta line represent the 5^{th}, 10^{th}, 15^{th}, 20^{th}, 25^{th}, and 30^{th} charge/discharge curves in Fig. 5b, respectively.

Fig. 6a and 6b show the charge/discharge profiles at different rates for the TiO_2 NT/NP heterostructure and the TiO_2 NT electrodes, respectively. Very flat charge/discharge plateaus at about 1.75 V and 1.9 V were observed in the charge/discharge curves of both the TiO_2 NT/NP heterostructure and the TiO_2 NT electrodes, which are related to the phase transition between the tetragonal and orthorhombic phases upon Li intercalation/deintercalation into/from anatase TiO_2, respectively[23, 24]. Moreover, because of the polarization of the electrodes, the discharge voltage plateaus of both the TiO_2 NT/NP heterostructure and the TiO_2 NT electrodes were shifted to lower voltages, while the charge voltage plateaus were shifted to higher voltages with increasing current densities. It is worthy noting that, at an high current density of 0.20 $mA \cdot cm^{-2}$, the voltage difference of the TiO_2 NT/NP heterostructure electrode between the charge and discharge voltage plateaus is smaller

than that of the TiO_2 NT electrode, indicating a smaller polarization and better rate capability of the TiO_2 NT/NP heterostructure electrode.

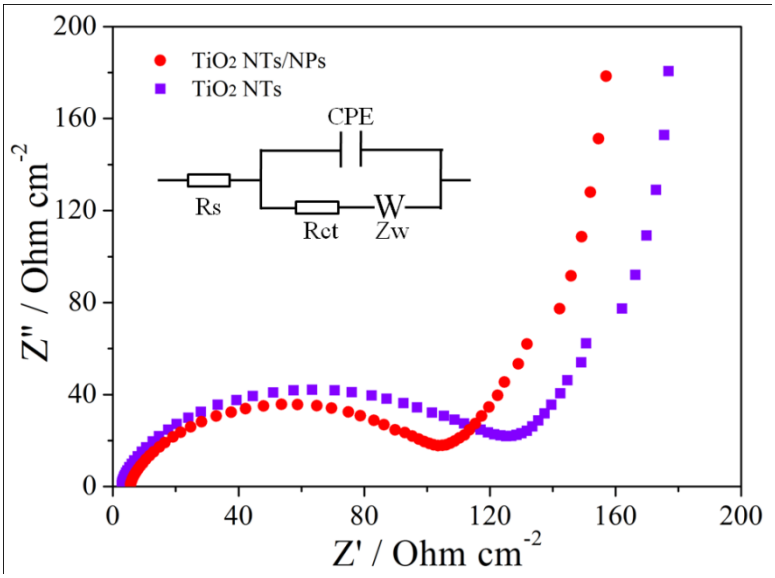

Fig. 7. Nyquist plot of the TiO_2 NT and the TiO_2 NT/NP heterostructure electrodes. Inset is the equivalent circuit used to fit the experimental impedance spectra.

In order to clarify the possible reason for the enhanced rate performance of the TiO_2 NT/NP heterostructure electrode, EIS, which is a powerful tool to provide information on electrode resistance, charge-transfer resistance and bulk resistance[5, 15], was used to evaluate the electrochemical characteristics of the two kinds of electrodes. The EIS spectra are showed in the form of Nyquist plots comprising a semicircle at high-to-medium frequence region, due to the charge-trasfer reaction at the electrolyte/electrode interface, and a straight line at low frequence region due to the diffusion of the Li^+ in the bulk of the electrode materials (Fig. 7)[39]. Meanwhile, the impedance data were also fitted with an equivalent circuit, including elements like

the electrode resistance (R_s), charge-transfer resistance (R_{ct}), constant phase elements (CPE), and Warburg diffusion element (Z_w), as shown in the inset of Fig. 7[33]. In this circuit, R_s stands for the ohmic resistance from the electrolyte, separator and electrodes, R_{ct} denotes the charge-transfer resistance between the active materials and the electrolyte, CPE represents the double layer capacitance, and Z_w is related to the diffusion of Li^+ into the electrode[23, 39]. From the semicircle diameter in the Nyquist plots, it can be observed that the R_{ct} of the TiO_2 NT/NP heterostructure electrode (55 Ω) is smaller than that of the TiO_2 NT electrode (65.8 Ω). This reveals a higher transfer rate of Li^+ in the TiO_2 NT/NP heterostructure electrode/electrolyte interface than in the TiO_2 NT electrode/electrolyte interface. The decreasing of R_{ct} of the TiO_2 NT/NP heterostructure electrode also results a reduction in the cell polarization, especially at high current density, which is in accordance with the results of charge/discharge tests.

Overall, the enhanced electrochemical performance of the TiO_2 NT/NP heterostructure electrode is thought to be related to the special heterostructure. Owing to the structural advantages of the TiO_2 NTs/NPs, with the TiO_2 NT cores providing straight pathways for electronic transport and TiO_2 NPs offering enhanced surface areas for lithium-ion insertion/extraction, the hierarchical architecture exhibits superior electrochemical performance, compared to its TiO_2 NT counterpart (Fig. 8).

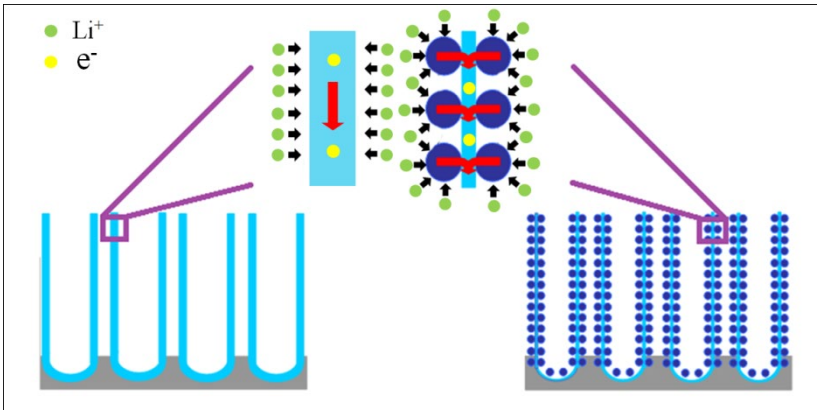

Fig. 8. Schematic illustration of electrochemical reaction mechanism of the TiO_2 NT (left) and the TiO_2 NT/NP heterostructure (right) electrodes.

4. Conclusions

A novel TiO_2 3D anode with aligned TiO_2 NT/NP heterostructure was developed by simply immersing as-anodized TiO_2 NTs into water, followed by further crystallization at 400 °C for 2h. The TiO_2 NT/NP heterostructure electrode displays higher areal capacity, better rate capability than its TiO_2 NT counterpart. The special microstructure of the TiO_2 NT/NP heterostructure electrode is the key to the enhanced electrochemical performance: the TiO_2 NT cores provide straight pathways for electronic transport, while the TiO_2 NPs offer enhanced surface areas for lithium-ion insertion/extraction. The newly developed TiO_2 NT/NP heterostructure electrode with enhanced areal capacity, rate capability as well as good cycle stability may have a great potential for lithium-ion microbattery applications.

Acknowledgements

This work was supported by the National Natural Science Foundation of China (No.51302219), the Specialized Research Fund for the Doctoral Program of Higher Education of China (No.20136102120024 and 20136102140001). The authors also appreciate the financial supports from the Research Fund of the State Key Laboratory of Solidification Processing (NWPU), China (Grant No.83-TZ-2013). This work was also supported by grants received from the Research Grants Council of the Hong Kong Special Administrative Region (PolyU5159/13E and M-PolyU503/13).

References

[1] M.M. Shaijumon, E. Perre, B. Daffos, P.L. Taberna, J.M. Tarascon, P. Simon, Nanoarchitectured 3D cathodes for Li-ion microbatteries, Adv. Mater. 22 (2010) 4978.

[2] S.K. Cheah, E. Perre, M. Rooth, M. Fondell, A. Harsta, L. Nyholm, M. Boman, T. Gustafsson, J. Lu, P. Simon, K. Edström, Self-supported three-dimensional nanoelectrodes for microbattery applications, Nano Lett. 9 (2009) 3230.

[3] H.G. Zhang, X.D. Yu, P.V. Braun, Three-dimensional bicontinuous ultrafast-charge and -discharge bulk battery electrodes, Nat. Nanotechnol. 6 (2011) 277.

[4] J.W. Long, B. Dunn, D.R. Rolison, H.S. White, Three-dimensional battery architectures, Chem. Rev. 104 (2004) 4463.

[5] K.Y. Xie, Z.G. Lu, H.T. Huang, W. Lu, Y.Q. Lai, J. Li, L.M. Zhou, Y.X. Liu, Iron supported C@Fe_3O_4 nanotube array: a new type of 3D anode with low-cost for high performance lithium-ion batteries, J. Mater. Chem. 22 (2012) 5560.

[6] G.F. Ortiz, I. Hanzu, T. Djenizian, P. Lavela, J.L. Tirado, P. Knauth, Alternative Li-ion battery electrode based on self-organized titania nanotubes, Chem. Mater. 21 (2008) 63.

[7] L. Baggetto, R.A.H. Niessen, F. Roozeboom, P.H.L. Notten, High energy density all-solid-state batteries: a challenging concept towards 3D integration, Adv. Funct. Mater. 18 (2008) 1057.

[8] P.L. Taberna, S. Mitra, P. Poizot, P. Simon, J.M. Tarascon, High rate capabilities Fe_3O_4-based Cu nano-architectured electrodes for lithium-ion battery applications, Nat. Mater. 5 (2006) 567.

[9] J.H. Pikul, H. Gang Zhang, J. Cho, P.V. Braun, W.P. King, High-power lithium ion microbatteries from interdigitated three-dimensional bicontinuous nanoporous electrodes, Nat. Commun. 4 (2013) 1732.

[10] K. Sun, T.S. Wei, B.Y. Ahn, J.Y. Seo, S.J. Dillon, J.A. Lewis, 3D printing of interdigitated Li-ion microbattery architectures, Adv. Mater. 25 (2013) 4539.

[11] J.F.M. Oudenhoven, L. Baggetto, P.H.L. Notten, All-solid-state lithium-ion microbatteries: a review of various three-dimensional concepts, Adv. Energy Mater. 1 (2011) 10.

[12] M. Guo, K.Y. Xie, J. Lin, Z.H. Yong, C.T. Yip, L.M. Zhou, Y. Wang, H.T. Huang, Design and coupling of multifunctional TiO_2 nanotube photonic crystal to

nanocrystalline titania layer as semi-transparent photoanode for dye-sensitized solar cell, Energy Environ. Sci. 5 (2012) 9881.

[13] C.T. Yip, H.T. Huang, L.M. Zhou, K.Y. Xie, Y. Wang, T.H. Feng, J.S. Li, W.Y. Tam, Direct and seamless coupling of TiO_2 nanotube photonic crystal to dye-sensitized solar cell: a single-step approach, Adv. Mater. 23 (2011) 5624.

[14] T. Djenizian, I. Hanzu, P. Knauth, Nanostructured negative electrodes based on titania for Li-ion microbatteries, J. Mater. Chem. 21 (2011) 9925.

[15] K.Y. Xie, J. Li, Y.Q. Lai, Z.A. Zhang, Y.X. Liu, G.G. Zhang, H.T. Huang, Polyaniline nanowire array encapsulated in titania nanotubes as a superior electrode for supercapacitors, Nanoscale 3 (2011) 2202.

[16] K.Y. Xie, J. Li, Y.Q. Lai, W. Lu, Z.A. Zhang, Y.X. Liu, L.M. Zhou, H.T. Huang, Highly ordered iron oxide nanotube arrays as electrodes for electrochemical energy storage, Electrochem. Commun. 13 (2011) 657.

[17] G.G. Zhang, W.F. Li, K.Y. Xie, F. Yu, H.T. Huang, A one-step and binder-free method to fabricate hierarchical nickel-based supercapacitor electrodes with excellent performance, Adv. Funct. Mater. 23 (2013) 3675.

[18] Y. Yang, D. Kim, P. Schmuki, Lithium-ion intercalation and electrochromism in ordered V_2O_5 nanoporous layers, Electrochem. Commun. 13 (2011) 1198.

[19] C.Y. Lee, K. Lee, P. Schmuki, Anodic formation of self-organized cobalt oxide nanoporous layers, Angew. Chem. Int. Ed. 52 (2013) 2077.

[20] N.A. Kyerematen, F. Vacandio, M.T. Sougrati, H. Martinez, J.C. Jumas, P. Knauth, T. Djenizian, Effect of Sn-doping on the electrochemical behaviour of TiO_2

nanotubes as potential negative electrode materials for 3D Li-ion micro-batteries, J. Power Sources 224 (2013) 269.

[21] H. Han, T. Song, E.K. Lee, A. Devadoss, Y. Jeon, J. Ha, Y.C. Chung, Y.M. Choi, Y.G. Jung, U. Paik, Dominant factors governing the rate capability of a TiO_2 nanotube anode for high power lithium ion batteries, ACS Nano 6 (2012) 8308.

[22] J.H. Kim, K. Zhu, J.Y. Kim, A.J. Frank, Tailoring oriented TiO_2 nanotube morphology for improved Li storage kinetics, Electrochim. Acta 88 (2013) 123.

[23] Z. Lu, C.T. Yip, L. Wang, H. Huang, L. Zhou, Hydrogenated TiO_2 nanotube arrays as high-rate anodes for lithium-ion microbatteries, ChemPlusChem 77 (2012) 991.

[24] W.H. Ryu, D.H. Nam, Y.S. Ko, R.H. Kim, H.S. Kwon, Electrochemical performance of a smooth and highly ordered TiO_2 nanotube electrode for Li-ion batteries, Electrochim. Acta 61 (2012) 19.

[25] Y. Wang, S.Q. Liu, K.L. Huang, D. Fang, S.X. Zhuang, Electrochemical properties of freestanding TiO_2 nanotube membranes annealed in Ar for lithium anode material, J. Solid State Electrochem. 16 (2012) 723.

[26] Y. Ren, Z. Liu, F. Pourpoint, A.R. Armstrong, C.P. Grey, P.G. Bruce, Nanoparticulate TiO_2(B): an anode for lithium-ion batteries, Angew. Chem. Int. Ed. 51 (2012) 2164.

[27] S.T. Myung, Y. Sasaki, S. Sakurada, Y.K. Sun, H. Yashiro, Electrochemical behavior of current collectors for lithium batteries in non-aqueous alkyl carbonate solution and surface analysis by ToF-SIMS, Electrochim. Acta 55 (2009) 288.

[28] E. Baudrin, S. Cassaignon, M. Koelsch, J.P. Jolivet, L. Dupont, J.M. Tarascon, Structural evolution during the reaction of Li with nano-sized rutile type TiO_2 at room temperature, Electrochem. Commun. 9 (2007) 337.

[29] D. Fang, K.L. Huang, S.Q. Liu, Z. Li, Electrochemical properties of ordered TiO_2 nanotube loaded with Ag nano-particles for lithium anode material, J. Alloys Compd. 464 (2008) L5.

[30] H.K. Sung, L.J. Woo, K.Y. Mook, L.J. Young, K.J. Ku, Nature of atomic and molecular nitrogen configurations in $TiO_{2-x}N_x$ nanotubes and tailored energy-storage performance on selective doping of atomic N states, Small 4 (2008) 1682.

[31] D. Liu, Y. Zhang, P. Xiao, B.B. Garcia, Q. Zhang, X. Zhou, Y.H. Jeong, G. Cao, TiO_2 nanotube arrays annealed in CO exhibiting high performance for lithium ion intercalation, Electrochim. Acta 54 (2009) 6816.

[32] D. Liu, P. Xiao, Y. Zhang, B.B. Garcia, Q. Zhang, Q. Guo, R. Champion, G. Cao, TiO_2 nanotube arrays annealed in N_2 for efficient lithium-ion intercalation, J. Phys. Chem. C 112 (2008) 11175.

[33] D.S. Guan, J.Y. Li, X.F. Gao, C. Yuan, Controllable synthesis of MoO_3-deposited TiO_2 nanotubes with enhanced lithium-ion intercalation performance, J. Power Sources 246 (2014) 305.

[34] L. Yu, Z. Wang, L. Zhang, H.B. Wu, X.W. Lou, TiO_2 nanotube arrays grafted with Fe_2O_3 hollow nanorods as integrated electrodes for lithium-ion batteries, J. Mater.Chem. A 1 (2013) 122.

[35] X.M. Wu, S.C. Zhang, L.L. Wang, Z.J. Du, H. Fang, Y.H. Ling, Z.H. Huang, Coaxial SnO_2@TiO_2 nanotube hybrids: from robust assembly strategies to potential application in Li^+ storage, J. Mater. Chem. 22 (2012) 11151.

[36] L.G. Xue, Z. Wei, R.S. Li, J.L. Liu, T. Huang, A.S. Yu, Design and synthesis of Cu_6Sn_5-coated TiO_2 nanotube arrays as anode material for lithium ion batteries, J. Mater. Chem. 21 (2011) 3216.

[37] H.S. Kim, S.H. Kang, Y.H. Chung, Y.E. Sung, Conformal Sn coated TiO_2 nanotube arrays and its electrochemical performance for high rate lithium-ion batteries, Electrochem. Solid State Lett. 13 (2010) A15.

[38] D.S. Guan, J.Y. Li, X.F. Gao, C. Yuan, Effects of amorphous and crystalline MoO_3 coatings on the Li-ion insertion behavior of a TiO_2 nanotube anode for lithium ion batteries, RSC Adv. 4 (2014) 4055.

[39] Y.P. Tang, X.X. Tan, G.Y. Hou, G.Q. Zheng, Nanocrystalline $Li_4Ti_5O_{12}$-coated TiO_2 nanotube arrays as three-dimensional anode for lithium-ion batteries, Electrochim. Acta 117 (2014) 172.

[40] J. Lin, X.L. Liu, M. Guo, W. Lu, G.G. Zhang, L.M. Zhou, X.F. Chen, H.T. Huang, A facile route to fabricate an anodic TiO_2 nanotube-nanoparticle hybrid structure for high efficiency dye-sensitized solar cells, Nanoscale 4 (2012) 5148.

[41] D.A. Wang, L.F. Liu, F.X. Zhang, K. Tao, E. Pippel, K. Domen, Spontaneous phase and morphology transformations of anodized titania nanotubes induced by water at room temperature, Nano Lett. 11 (2011) 3649.

[42] N. Liu, S.P. Albu, K. Lee, S. So, P. Schmuki, Water annealing and other low temperature treatments of anodic TiO_2 nanotubes: a comparison of properties and efficiencies in dye sensitized solar cells and for water splitting, Electrochim. Acta 82 (2012) 98.

[43] G.F. Ortiz, I. Hanzu, P. Knauth, P. Lavela, J.L. Tirado, T. Djenizian, TiO_2 nanotubes manufactured by anodization of Ti thin films for on-chip Li-ion 2D microbatteries, Electrochim. Acta 54 (2009) 4262.

[44] K. Zhu, Q. Wang, J.H. Kim, A.A. Pesaran, A.J. Frank, Pseudocapacitive lithium-ion storage in oriented anatase TiO_2 nanotube arrays, J. Phys. Chem. C 116 (2012) 11895.